FLUCTUATIONS IN TENSION DURING CONTRACTION OF SINGLE MUSCLE FIBERS

JULIAN BOREJDO AND MANUEL F. MORALES, *Cardiovascular Research Institute, University of California, San Francisco, California 94143 U.S.A.*

ABSTRACT We have searched for fluctuations in the steady-state tension developed by stimulated single muscle fibers. Such tension "noise" is expected to be present as a result of the statistical fluctuations in the number and/or state of myosin cross-bridges interacting with thin filament sites at any time. A sensitive electro-optical tension transducer capable of resolving the expected fluctuations in magnitude and frequency was constructed to search for the fluctuations. The noise was analyzed by computing the power spectra and amplitude of stochastic fluctuations in the photomultiplier counting rate, which was made proportional to muscle force. The optical system and electronic instrumentation together with the minicomputer software are described. Tensions were measured in single skinned glycerinated rabbit psoas muscle fibers in rigor and during contraction and relaxation. The results indicate the presence of fluctuations in contracting muscles and a complete absence of tension noise in either rigor or relaxation. Also, a numerical method was developed to simulate the power spectra and amplitude of fluctuations, given the rate constants for association and dissociation of the cross-bridges and actin. The simulated power spectra and the frequency distributions observed experimentally are similar.

INTRODUCTION

The current hypothesis of how muscle works asserts that a contractile force is a superposition of mechanical impulses delivered by myosin cross-bridges to sites on actin filaments. The direct substantiation of this assertion may prove difficult for many reasons and especially because of asynchrony among the impellers. An analysis of stochastic fluctuations associated with the cyclic mechanochemical interactions between cross-bridges and actin sites circumvents the asynchrony problem and thus may yield evidence we seek. The hypothesis anticipates that during the development of a steady-state active tension there will be tension fluctuations around the mean, arising from statistical variations in operation of impellers acting in any time interval. In the present work we search for and find such tension fluctuations and our analysis shows that they are mainly composed of frequencies in the 0–4 Hz range. There is as yet no sure way to exclude all possible artifactual origins of this observation, but two considerations suggest that the fluctuations that we detect may indeed arise from cross-bridge cycling. Firstly, in solution, myosin saturated with actin at room temperature catalyzes ATP hydrolysis at a rate that lies within the observed frequency range.[1] Secondly,

[1]We are speaking here of similarity between the frequencies. We cannot expect numerical identity because in the fiber external force affects certain transitions (as discussed by T. C. Hill [9]) and perhaps also because of the fiber-solution differences discussed by Weber and Murray (28).

numerical calculations designed to simulate the behavior of an A. F. Huxley-type of cross-bridge model with plausible numerical values assigned to its parameters show that the shape of the frequency distribution ("power spectrum") that the model generates closely resembles the shape of the power spectrum characterizing the observed fluctuations.

Fluctuation analysis has been applied to several situations of biological interest (1–3). As regards active muscle, its application was pioneered by F. D. Carlson and his associates (4–6), who from quasielastic light scattering deduced the existence of fluctuations that they assigned to the motions of structures considerably larger than cross-bridges. Spectroscopic methods have not as yet been applied to the problem of fluctuation in the mean sarcomere length, although such fluctuations have been predicted theoretically (7). We chose to study tension fluctuations because there exists a well-established model relating these to fluctuation in the number of active cross-bridges and because, with appropriate instrumentation (see below), tension fluctuations can be straightforwardly and accurately measured in skinned single fibers.

For a muscle model that would simulate fluctuations of the sort that we propose to observe in muscles, we chose a variant of the original A. F. Huxley model (8), because we knew what numerical values could be assigned to its parameters in order to account successfully for a variety of contractile phenomena. Hill (9) and Chen and Hill (10) have discussed the actin-myosin-ATP interactions underlying Huxley-type models and derived analytical expressions for the power spectrum of force fluctuations. Our treatment of the stochastic fluctuations recognizes Hill's formalism and takes advantage of a Monte Carlo method for probabilistic simulation of a distribution of cross-bridges in active muscle to evaluate the power density spectrum of fluctuations. This approach proved useful in predicting the effect of experimental variables on the shape of the power spectra.

METHODS

For the detection of small force fluctuations one should employ a sensitive tension transducer with a frequency response broad enough to cover the expected range of frequencies (Fig. 11). At the same time it is advantageous to be able to offset the DC part of the tension, thus effectively extending the dynamic range of the device. Such an offset allows one to measure the absolute rather than the relative fluctuations, which in turn can be made large by increasing the number of active cross-bridges (i.e., muscle tension). These considerations prompted construction of an electro-optical transducer shown schematically in Fig. 1.

Optical

A beam of light from a battery-operated light bulb (S) is focused by a lens (L_1), attenuated by a set of neutral density filters (ND), and directed by mirrors (M) into the condenser of a Zeiss standard GFL microscope (Carl Zeiss, Inc., New York). The muscle fiber is mounted in an experimental chamber (EC) resting on the microscope stage. The cell is similar in design to the one previously described (11,12): the muscle fiber is mounted between a solid support and an elastic glass arm, which has an opaque flag (FL) attached at the end (Fig. 1B). Another lens (L_2) and an adjustable diaphragm (D) focus the light into the flag. The deflection of the arm is calibrated in terms of the contractile force according to Eq. 2 (see below). The microscope

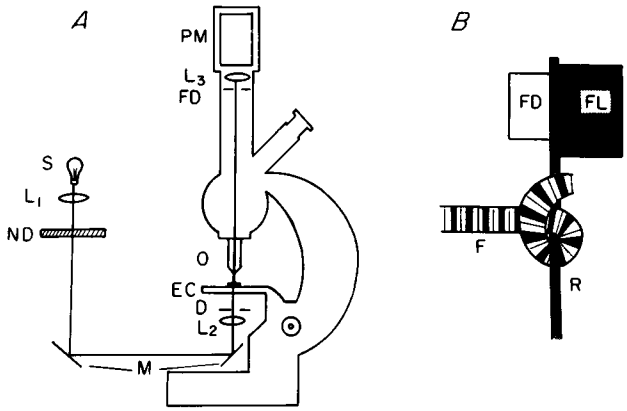

FIGURE 1 Schematic diagram of the electro-optical tension transducer. The whole assembly diagrammed in A rests on an optical table isolated from floor vibrations. The dimensions of the image of the field diaphragm in B are 2 × 2 μm.

objective 0 (40 × water immersion, numerical aperture [NA] = 0.75) projects the image of the flag into the field diaphragm (FD) positioned at the back focal plane of the objective. An adjustable diaphragm selects the central area of the field of view of the objective, and the lens L_3 (40 × objective, NA = 0.65) expands the image of the diaphragm and projects it into the photomultiplier tube (PM) (RCA 8850, RCA Co., Harrison, N.J.). Thus the extremely small variations in the position of the flag are translated into large changes in the photomultiplier current. Sensitivity of detection is critically influenced by the size of the field diaphragm in the direction of the arm movement. At around 80 μm the diffraction limit is reached and consequently a slit of this size was used in all experiments.

Electronics and Data Processing

Fig. 2 illustrates the electronic circuitry employed to process the photomultiplier signals. The output of the photomultiplier is amplified by a 20 × DC amplifier (Lawrence Research Laboratories, Berkeley, Calif., Model 4421 P) and processed by a discriminator (LeCroy Research Sys-

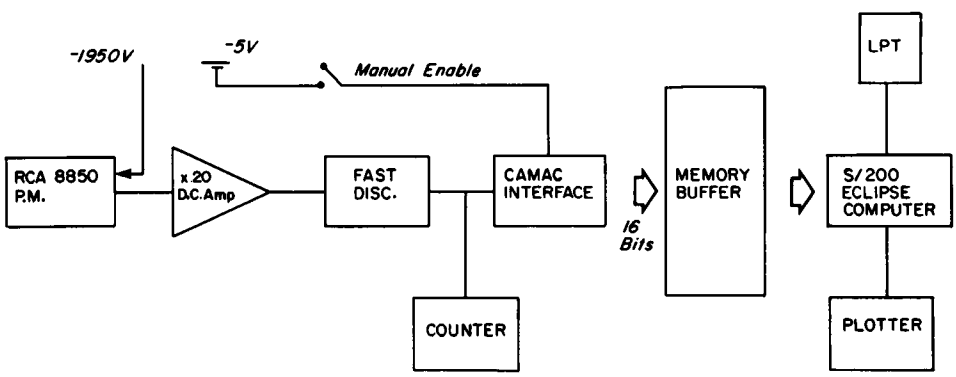

FIGURE 2 Electronic circuitry used to process the displacement signal. For explanation see text. Manual enable is a remote control of the CAMAC gate to allow one to begin accumulation of data while observing the muscle under the microscope.

tems, West Nyack, N.Y., Model 620 AL) to produce a series of identical pulses corresponding to detection of single photons. A 12 MHz Hex Scaler (Lawrence Research Laboratories, Model 4321 P2) counts the rate of arrival of photons and is used to set the incident light intensity. The output of the discriminator is fed into a CAMAC Quad Scaler QS 100 computer interface (Standard Engineering Co., Fremont, Calif.) which produces a continuous string of 16-bit (integer) numbers, each number representing the photomultiplier counting rate in the time interval (referred to as bin width) defined by the user. The bin width is typically fixed at 20 ms. The string of data is stored in contiguous files on a computer disk and subsequently accessed for analysis. Each file consists of 4,096 bins and is a digital record of tension developed during 81.92-s-long time interval. The file is subdivided into four sweeps 1,024 bins long (20.48 s) and each sweep is analyzed separately. The signal contained in each sweep has a nonzero mean value and more generally is nonstationary because of the creep in muscle tension during tetanus plateau. A stationary signal with zero mean is constructed for spectral analysis by subtracting the systematic trend. A straight line trend is estimated by the least-squares method, and obviously nonlinear data are rejected from further analysis. "Detrended" data (1,024 points) are extended to 2,048 points by padding with zeros and first and last 64 points are tapered with a "cosine bell" window (13). A fast Fourier transform (FFT, Cooley-Tukey algorithm, ref. 14) is applied to the resulting sequence of points to produce an amplitude spectrum, which is then squared to give a power density spectrum. The spectrum is smoothed by computing the autocorrelation function of the original data and applying a triangular Bartlett window to the first and last K points of the 2,048-point sequence (13). K is typically 256. The "windowed" autocorrelation function is forward-transformed by the FFT and plotted as a smoothed power density curve. The computer also calculates the tension drift rate, the rms fluctuation, and the expected rms fluctuation of the signal. These are calculated as follows: the primary measurement is a rate of photon arrivals. It is found that these rates are normally distributed and the "observed" rms deviation is straightforwardly:

$$<\delta\eta>_{\text{obs}} = \left(\sum_{i=1}^{N} \delta\eta_i^2/N\right)^{1/2},$$

where $\delta\eta_i = \eta_i - \bar{\eta}_i$ and $\bar{\eta}_i$ is the mean rate appropriate to the time at which η_i is measured.

On the other hand, inherent in the counting process itself is a dispersion which increases as a square root of the mean rate (15). If this counting error were the only source of dispersion in the N rate measurements, one would expect a deviation:

$$<\delta\eta>_{\text{exp}} = (1/N)\left(\sum_{i=1}^{N} \bar{\eta}_i^{1/2}\right). \quad (1)$$

An important comparison below will be that between $<\delta\eta>_{\text{obs}}$ and $<\delta\eta>_{\text{exp}}$, referred to as observed and expected fluctuation.

Apparatus Performance

The apparatus response was linear within few percent over the entire operating range. The sensitivity was measured by looking for variations in the rms fluctuation and in spectral shape with amplitude of microscopic oscillations imposed on the flag. The flag was attached to a needle of a milliammeter driven by a sinusoidally varying voltage from a high impedance power supply. In the power spectrum 10 nm oscillations were easily resolved (Fig. 3A). The practical limit of sensitivity was reached at 1 nm amplitude (although with longer data collection time the limit can probably be further reduced) (Fig. 3B).

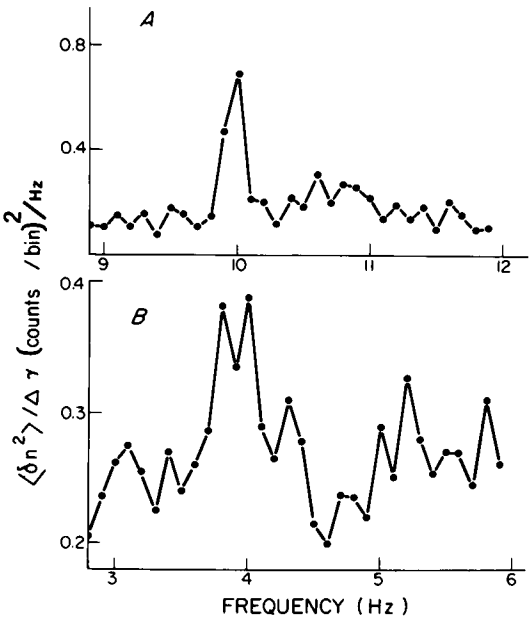

FIGURE 3 Power spectrum of sinusiodal vibrations imposed on a flag by an external oscillator. A: 10 Hz oscillations, 100 Å p-p amplitude, 10 ms bin width, 40.96-s data collection time. B: 4 Hz oscillations, 10 Å p-p amplitude, 10 ms bin width, 163.84 sec data collection time. Counting rates in A and B were 1.556×10^6/s and 3.237×10^5/s, respectively. δn is a fluctuation in counting rate in counts per bin width.

Design Considerations

The ultimate sensitivity of the apparatus in terms of force is determined by the compliance of the arm to which the fiber is attached. We ask now whether it is advantageous to use an arm of high compliance and to allow the muscle to develop only a small force, or whether it is better to employ a low-compliance arm and generate large tensions. Let the fiber length be l and the maximum length change during contraction that one is willing to tolerate be Δl. From Table II we compute that the absolute rms fluctuation decreases slowly with increasing number of half-sarcomeres. For simplicity we estimate that the absolute force fluctuations can be approximated by the empirical (based on Table II) equation $\langle \delta F^2 \rangle^{1/2} = yn^{1/2}/1.2 \log N$, where n is the number of cross-bridges per half-sarcomere, $N \geq 2$ is the number of half-sarcomeres and $y = 1.6$ pN the average force per cross-bridge. If $F = ny$ is the force developed by the muscle, then the transducer compliance is:

$$C = \Delta l/yn, \tag{2}$$

and the fluctuations in displacement d are:

$$\langle \delta d^2 \rangle^{1/2} = \Delta l\, yn^{1/2}/(1.2 \log N)\, yn = A \Delta l n^{-1/2}, \tag{3}$$

where A is a constant. Since the displacement of the arm Δl can be offset by moving the cell across the field of view of the microscope, it does not contribute to a DC signal. Thus within the limit of practicability the transducer arm should be as compliant as possible, and the muscle should develop the largest tension possible, but not larger than $\Delta l/C$.

The compliance of the arm and its characteristic frequency are given by (16, 17)

$$C = l_a^3/3IE, \tag{4}$$

$$\omega = (3.52/l_a^2)(EI/\rho S)^{1/2}, \tag{5}$$

where l_a is the length of the arm, E its Young modulus, I the moment of inertia about its long axis, S the cross-sectional area, and ρ its density. For an arm of cylindrical shape with radius r:

$$C = 4l_a^3/3r^4E, \tag{6}$$

$$\omega/2\pi = \nu = (3.52r/4\pi^{3/2}l_a^2)(E/\rho)^{1/2}. \tag{7}$$

The largest possible compliance is determined by the smallest practical arm diameter. Below $r = 15$ μm, the mounting of the fiber becomes too difficult and with a typical l_a at a point of muscle attachment of 7 mm, $C = 129$ μm/μN and $\nu = 7.9$ Hz (E for glass $= 7 \times 10^6$ N/cm^2). Setting $\Delta l/l$ somewhat arbitrarily at .2 and a typical l at 1 mm, give $n = 1 \times 10^6$ and $F = 1.6$ μN. The sensitivity of the apparatus is thus $10 \times 10^6/1.290 \times 10^7 = 7.8$ pN. Such sensitivity together with a reasonable frequency response gives this transducer characteristics not easily matched by conventional stress gauges.

The optimal muscle tension is smaller than the maximum isometric force by a factor of about 200. To obtain such low tensions, the fiber was either extracted with Hasselbach-Schneider (HS) solution or dissected down to a small myofibrilar bundle 3–5 μm in diameter (see below).

Fiber Preparation and Handling

For several reasons glycerinated muscle fibers were a logical choice for experimental material. Firstly they eliminate the need for electrical stimulation and possible complications associated with the use of an AC stimulating signal (18). Secondly, they can sustain prolonged contraction with little tension drift (creep) compared to live fibers (19) (but see Results). Finally, the maximum tension generated by glycerinated fibers is easily adapted to other requirements, either by extraction of myosin or by mechanical dissection to a small myofibrilar bundle (20).

Fresh strips of rabbit psoas muscle were glycerinated according to conventional procedure (11) and stored for 2–8 wk before use. Before each experiment the fibers were equilibrated with rigor solution (80 mM KCl, 5 mM $MgCl_2$, 2 mM EGTA, 5 mM Na phosphate buffer, pH = 7.0); a single fiber was dissected and then skinned by splitting it lengthwise with a pair of sharpened jeweler's tweezers as previously described (11). Mounted fibers were typically 30–50 μm in diameter and 1 mm in length. The desired reduction in tension was achieved by a 2-min extraction of the fibers with the modified HS solution (0.6 M KCl, 10 mM Na pyrophosphate, 2 mM $MgCl_2$, 0.1 M Na phosphate buffer, pH = 6.4). Skinning assured good accessibility by the solutes and, in contrast to the unskinned fibers, short extraction with HS solution was enough to abolish more than 99% of the tension. Stimulation was achieved by the application tion of contracting solution (80 mM KCl, 5 mM $MgCl_2$, 0.1 mM $CaCl_2$, 5 mM ATP, 5 mM Na phosphate buffer, pH = 7.0). Relaxing solution had the same composition except that Ca^{2+} was replaced by 2 mM EGTA. All experiments were carried out at room temperature (20°C).

RESULTS

Tension Creep during Contraction

Even though glycerinated fibers exhibited little tension creep in comparison with live fibers, the drift in force constituted a significant technical problem at the levels of

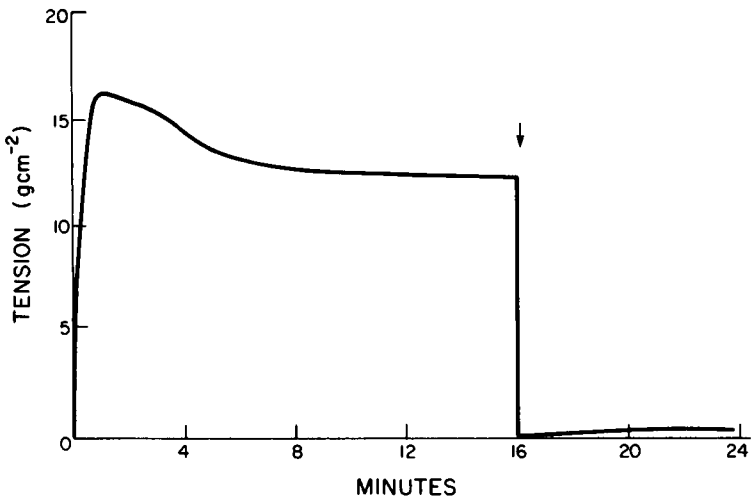

FIGURE 4 The time-course of tension development in a skinned muscle fiber treated with HS solution. Fiber diameter was 46 μm (cross-sectional area assumed circular). Contracting solution added at time 0. Arrow marks the time of quick release to zero tension.

sensitivity employed here. Fig. 4 shows the tension-time curve for a typical fiber preparation, that is, a single fiber extracted with HS solution. After reaching a maximum shortly after the beginning of stimulation, the tension begins to decline and attains a quasi-steady value within 10 min. Since it takes at least 20 s to collect the data, the tension cannot creep at a rate exceeding 0.78 nN/s or the flag will sweep across the field of view defined by the diaphragm before the measurement is completed. Such low rates of creep are not attained until 3–5 min after the beginning of contraction and so the data collection was initiated at this time. When the fiber tension is quickly released at this time, the recovery of force is slower than the original development and is incomplete (20% of maximum, not shown in Fig. 4). 10 min after the onset of contraction and later, the redevelopment of force is very slow and insignificant (Fig. 4). Thus it appears that a large part of the total tension at the time of measurement may be contributed by rigor complexes between actin and myosin.

To separate the creep from the superimposed fluctuations of interest, a fit to the data has to be made and the two have to be subtracted to give a set of corrected points stationary in time and with zero mean (see Methods). Fig. 5 shows the tension-time curves for rigor and contracting muscle during the data collection time. In this and many other experiments the straight line fit was clearly a good one, at least within each sweep (1,024 bins). As described in Methods, least square lines are fitted to the sweeps independently. Only those sweeps in which tension signals appeared to change linearly with time were processed further. As an example, consider sweep 3 (bins 2,048–3,072) of Fig. 5. It is shown again after detrending in Fig. 6. Clearly, the detrended signal does not show any obvious systematic deviations from the mean. Further, the histo-

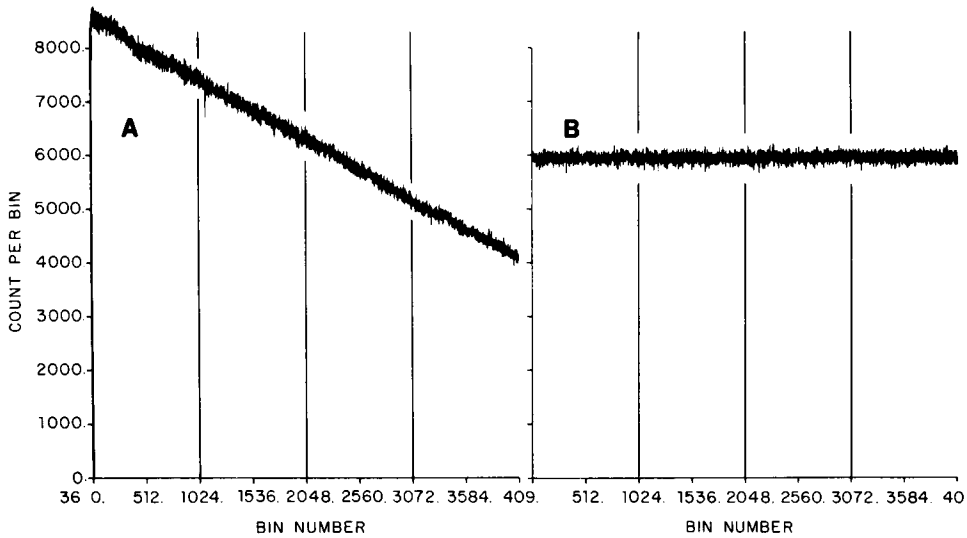

FIGURE 5 Tension-time curves for contracting (A) and rigor (B) muscle. Counting rate (ordinate) is proportional to flag displacement and hence to the tension. The abscissa is proportional to time (20 ms/bin). Vertical lines divide the record into sweeps.

gram of fluctuations from the mean (Fig. 7) served as a criterion for accepting the data for analysis. The symmetry of the histogram was a necessary (though not sufficient) condition for analyzing the data. Thus, for example, the first sweep in Fig. 5A (bins 0–1,024) was not analyzed because the sudden tension jump produced an asymmetric histogram. Similarly, the second sweep (bins 1,024–2,048) was omitted because of the large transient at the beginning. In the example shown only sweeps 3 and 4 (bins 2,048–3,072 and 3,072–4,096) were analyzed according to the procedure described in Methods.

Power Spectra of Force Fluctuations in Rigor and Contraction

Fig. 8 A shows the typical power spectrum of the signal contained in a 20.48-s-long sweep of tension record of contracting muscle. The expected and measured fluctuations during this time interval were 75.7 and 81.3 counts/bin, respectively. Fig. 8 B shows the spectrum of the rigor force signal contained in one sweep of tension record of rigor muscle. In this case the power spectrum is flat while the expected and observed fluctuations were 77.1 and 78.5 counts/bin, respectively.

The power spectra shown in Fig. 8 are very noisy (at any frequency the variance of the spectrum equals its mean value: cf. ref. 13), and consequently some of their features may be overlooked. The application of a smoothing procedure (Bartlett's window 256 bins wide) reduces the variance by a factor of approximately 8; the resulting smoothed power spectra for contracting and rigor muscle are shown in Fig. 9 A and B, respectively. Apart from the low frequency broadening, there were no secondary maxima within the range of frequencies investigated.

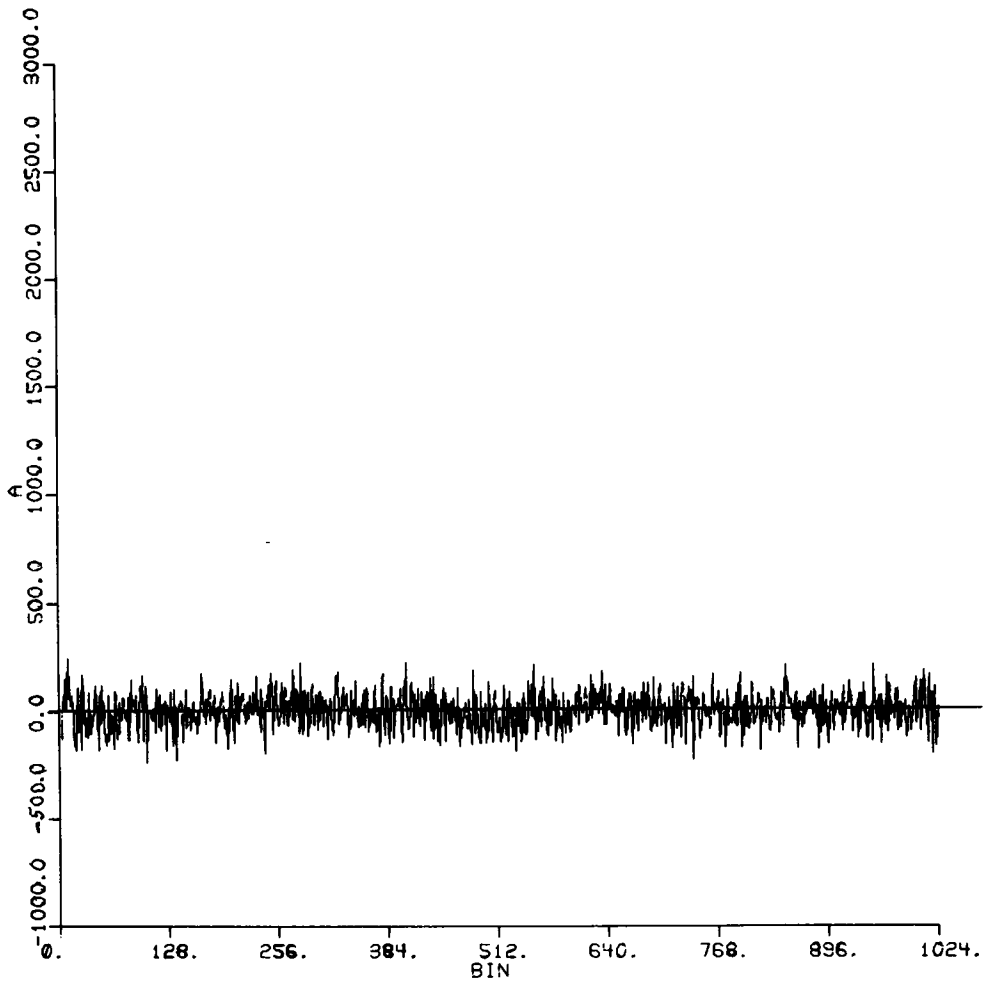

FIGURE 6 Detrended signal contained in bins 2,048–3,072 of Fig. 5A, showing lack of systematic deviations from the mean.

In all cases studied, contracting muscles gave rise to spectra similar to the ones illustrated in Figs. 8 A and 9 A. The amount of broadening depended on the time of data collection after the application of contracting solution: the later the data collection interval, the narrower the spectrum. In all cases muscles in rigor gave completely flat power spectra. The results of 13 experiments are summarized in Table I: the increase in fluctuation magnitude in a control experiment (no muscle) is due to the vibration of the free transducer arm. The spectrum of these vibrations was flat everywhere except at $\nu = 6.2$ Hz, where there was a sharp peak (corresponding to the characteristic frequency of the arm vibrating in water). However, even a small stress applied to the arm abolished the fluctuations completely, and consequently in all rigor experiments a small resting tension was applied to the fiber.

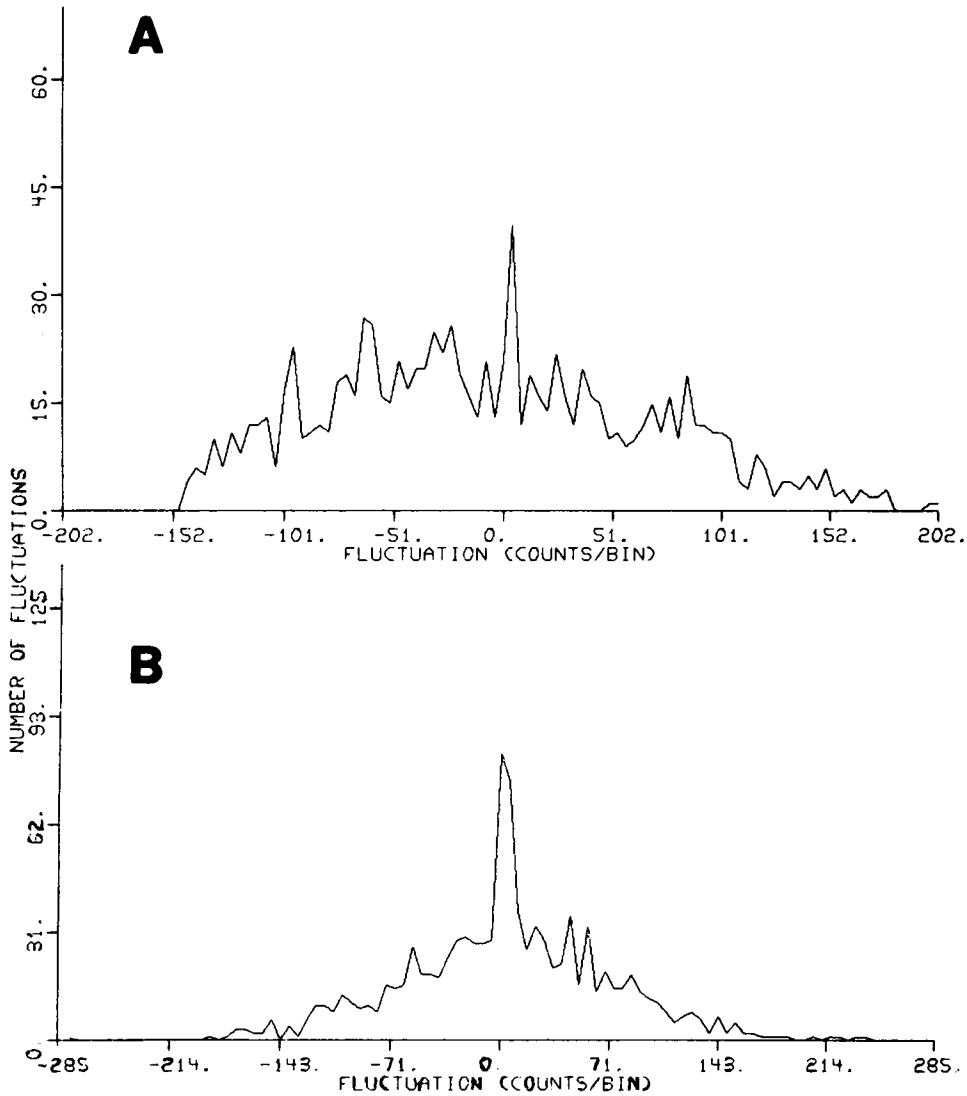

FIGURE 7 Histogram of fluctuations used to establish the validity of a straight line fit to the signal. A: gently sloping, simulated parabolic signal of the form $0.001\ (x + 500)^2$ ($x = 1, \ldots, 1{,}024$) with random fluctuations superimposed on it, showing asymmetry which would exclude it from analysis. B: actual experimental signal (Fig. 5A, sweep 3).

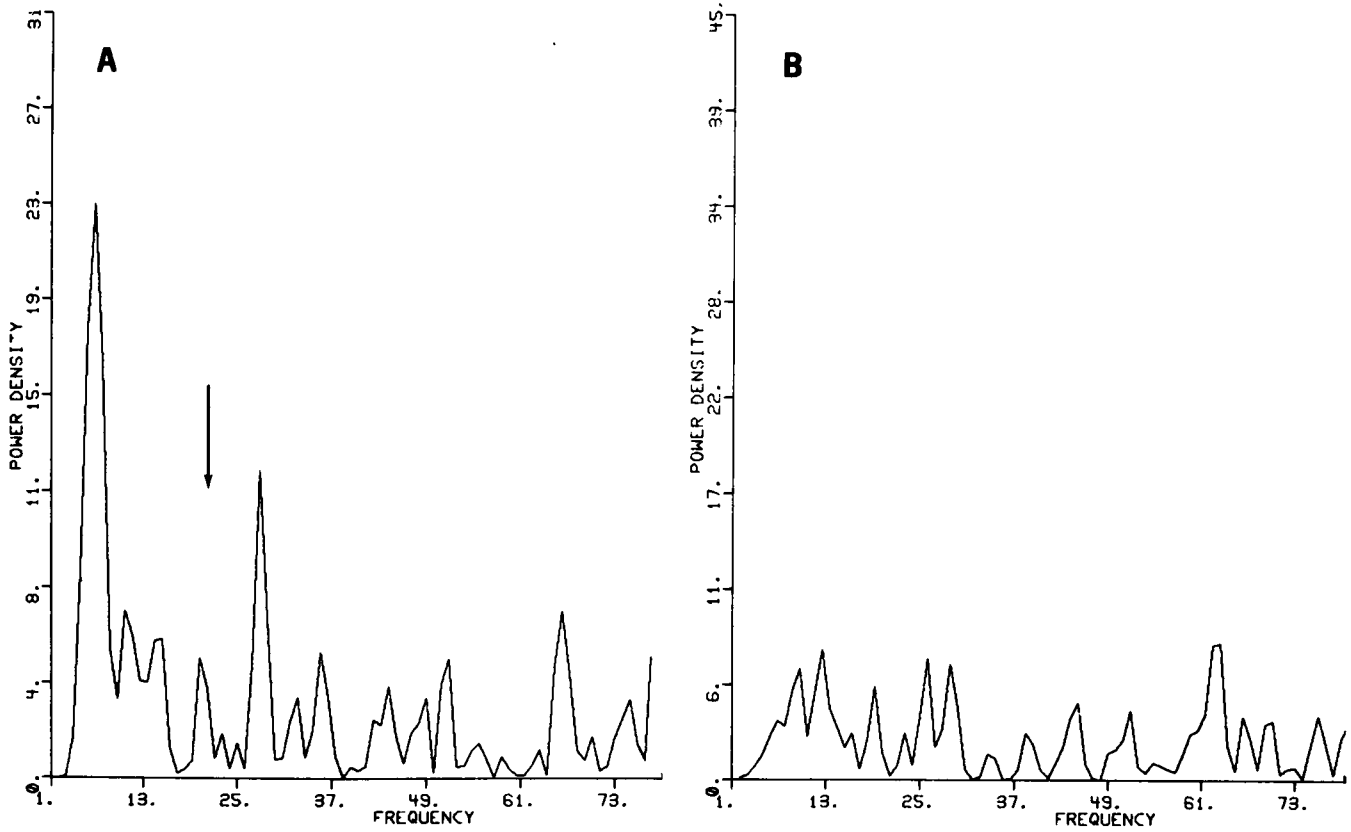

FIGURE 8 Power spectra of tension signal A: contraction data obtained from 20.48-s-long period (sweep 3, Fig. 5A) B: rigor, data obtained from 20.48-s-long period (sweep 2, Fig. 5B). The ordinate: power density in $(\text{counts/bin})^2$ per hertz. The abscissa: frequency with 20.48 corresponding to 1 Hz. The square root of the number corresponding to the area under the power density curves is the rms value of the original data sequence. The arrow marks the frequency of 1 Hz.

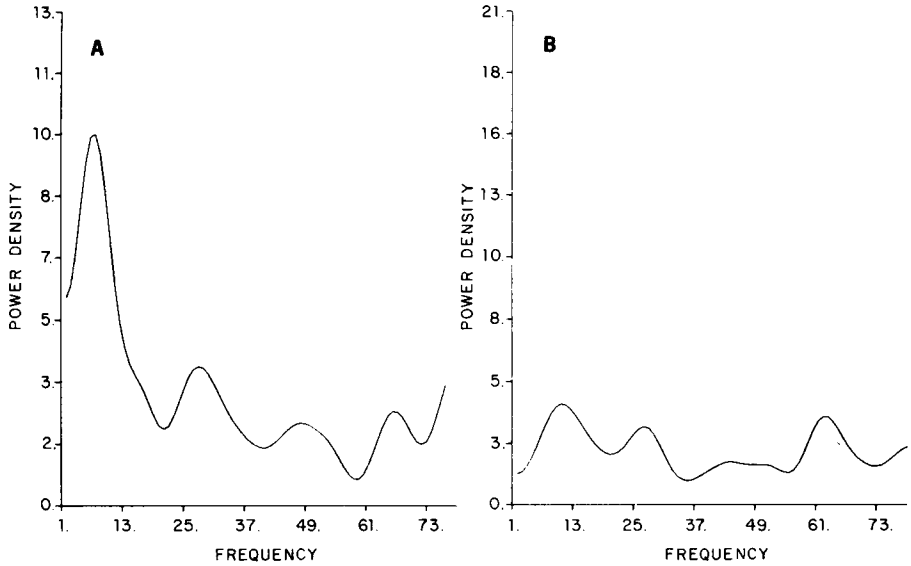

FIGURE 9 Smoothed power spectra of Fig. 8. A, contraction; B, rigor. Smoothing achieved by applying a Bartlett's window 256 bins wide. Ordinate: power density in units of (counts/bin)^2 per hertz. The abscissa: frequency with 20.48 corresponding to 1 Hz.

TABLE I

THE FORCE FLUCTUATIONS AND THEIR FREQUENCY DISTRIBUTION IN SINGLE FIBERS

Experiment	Conditions	Drift rate	Expected fluctuation	Observed fluctuation	Broadening	Observed fluctuation / Expected fluctuation
		pN/s	*counts/bin*	*counts/bin*	*Hz*	
26	Rigor	0	62.4	63.3	0	1.01
26	Contraction	75	48.7	156.6	1.3	3.21
27	Rigor	18	69.5	71.6	0	1.03
27	Contraction	398	71.0	100.8	1.2	1.42
27a	Rigor	4	62.3	64.9	0	1.04
27a	Contraction	173	68.4	83.3	0.9	1.22
28	Rigor	3	65.3	65.0	0	0.99
28	Contraction	519	69.4	117.4	0.5	1.69
32	Rigor	34	59.1	62.5	0	1.06
32	Contraction	189	85.6	113.3	3.5	1.32
32a	Rigor	34	55.8	58.2	0	1.04
32a	Contraction	188	71.7	83.6	2.5	1.17
33	Rigor	0	77.1	78.5	0	1.02
33	Contraction	121	75.7	81.3	1.5	1.07
33a	Rigor	1	77.2	77.3	0	1.00
33a	Contraction	118	67.8	73.4	2.0	1.08
	No muscle	15	46.8	109.7	—	2.34
	Relaxation	1	41.2	42.8	0	1.04

Bin width was 20 ms in all experiments. Broadening was defined as the highest frequency component distinguishable above the background on the plots of the type shown in Fig. 9A.

THE MUSCLE MODEL

Force Generation

Our model is designed to function in our particular experiments. The "muscle" consists of many serially arranged "half-sarcomeres" acting against a spring of fixed compliance (the "transducer"). A half-sarcomere is at once a force generator and a series elastic component. Force is generated by a mechanism of the sort first proposed by A. F. Huxley (8) and modified by Hill et al. (21). In this mechanism the force results from summing interactions between regularly spaced cross-bridges along the thick filament and regularly (but differently) spaced attachment sites on the thin filament. An essential feature of this type of model is that the number of operating cross-bridges is independent of sarcomere length and hence it is not unstable in the sense discussed by Jackson and Oplatka (7). If a cross-bridge is detached it contributes no force, but if it is attached it contributes a force, $f = kx$, where k is a stiffness constant and x is the axial displacement from the axial coordinate at which it exerts no force. In the Huxley treatment $n(x)\,dx$ is the number of cross-bridges whose displacements lie between x and $x + dx$. The force exerted by all the bridges in a single half-sarcomere is therefore the integral over all x of $n(x) \cdot kx dx$. A differential equation relates the time rate of change of n to the minimal set of rate constants. In the original Huxley treatment (8), these constants were f for attachment and g for detachment; Hill and his colleagues (21) later pointed out that for conceptual, if not for practical computational reasons, one must use f and f' for attachment to and detachment from a bound state and g and g' for detachment from and attachment to a chemically different bound state. When the Huxley treatment is going to be applied numerically—as it is here—the differential equation for n need not be solved analytically. Following Brokaw (22), a future n can be calculated from a present n by a Monte Carlo method. Given the probabilities for detachment, $p_1(x)$ and $p_2(x)$, and for attachment, $p_3(x)$ and $p_4(x)$, as well as $n(x)$ in interval Δt_τ, we compute $n(x)$ at $\Delta t_{\tau+1}$, by asking for each cross-bridge in turn whether $p(x)$ is greater than a random variable selected from the range 0 to 1. If the answer is yes, then the cross-bridge executes the transition proposed; if no, then its status remains unchanged. The p's are taken as in ref. 21:

$$\begin{aligned} p_1(x) &= a(x)(1 - e^{-\gamma\Delta t})/[a(x) + b(x)] \\ p_2(x) &= g(x)/a(x) \\ p_3(x) &= b(x)(1 - e^{-\gamma\Delta t})/[a(x) + b(x)] \\ p_4(x) &= f(x)/b(x), \end{aligned} \tag{8}$$

where

$$\begin{aligned} a(x) &= f'(x) + g(x) \\ b(x) &= f(x) + g'(x) \\ \gamma(x) &= a(x) + b(x), \textit{ and} \\ \Delta t &= \textit{length of the time interval.} \end{aligned} \tag{9}$$

Computational Procedures

For force generation in the ith (of N) half-sarcomere of the series (the "muscle"), a vector, $\mathbf{V}_i$, plays the role of Huxley's "$n(x)$". The jth component of $\mathbf{V}_i$ refers to the jth cross-bridge in the ith half-sarcomere. Let the instantaneous distance between cross-bridge 1 and the site 1 on the thin filament be σ and the spacings on the thick and thin filaments be S_M and S_A, respectively. The jth cross-bridge is therefore at axial distance jS_M along the thick filament. The thin filament site nearest in axial distance to the jth cross-bridge is the j_Ath, $x_j = jS_M - j_AS_M + \sigma$, and j_A is the integer that minimizes $|x_j|$. The jth component of $\mathbf{V}_i$ is zero or nonzero depending on whether the jth cross-bridge is detached or not, and the number of attached cross-bridges is M_i. Time is split up into small equal intervals numbered, $1, 2, \ldots \tau, \ldots$ The quantities, $\mathbf{V}_i$, x_j, M_i, etc. are functions of τ. At $\tau = 0$ we assume that $\mathbf{V}_i = 0$ for all i. As τ increases, $\mathbf{V}_i$ evolves stochastically, through repeated application of the Monte Carlo method, and so does the tension, T, felt by the transducer in series with the muscle (see below for the calculation of T from the $\mathbf{V}_i$). The $\mathbf{V}_i$ and T finally reach stationary levels. However, in the stationary state T is not precisely constant but fluctuates around a mean value. What we want is the distribution of frequencies underlying these fluctuations.

The vector, $\mathbf{V}_i(\tau + 1)$, specifies the extensions of the $M_i(\tau + 1)$ attached cross-bridges in half-sarcomere i. These bridges are in parallel, so there is also specified an ith force,

$$f_i = k\Sigma x_j, \tag{10}$$

where k is the Young's modulus divided by the rest length of a cross-bridge, and the summation is over the M_i attached cross-bridges. The length of sarcomere is not specified in this simple model, but we assume a sarcomeric structure such that if this system of variously stretched cross-bridges responds to external forces, each bridge will suffer the *same* change of length, say λ_i. In particular, if the external tension balancing the suddenly decided f_i increases to what will be the final equilibrium tension during interval, $\tau + 1$, viz., $T^{eq}(\tau + 1)$, then,

$$\lambda_i = [T^{eq}(\tau + 1) - f_i(\tau + 1)]/M_ik. \tag{11}$$

For the muscle as a whole, the change in length will be the algebraic sum of the N terms, λ_i. Since the experiment is performed under "isometric" conditions, the change in length of the transducer will therefore be,

$$\lambda_s = -\sum_{i=1}^{i=N} \lambda_i \tag{12}$$

The transducer has a stiffness, k_s, and was in equilibrium with $T(\tau)$; therefore, in adjusting to $T^{eq}(\tau + 1)$ it suffers a change in length,

$$\lambda_s = [T^{eq}(\tau + 1) - T^{eq}(\tau)]/k_s. \tag{13}$$

Eqs. 10–13 provide the recursion necessary to calculate $T^{eq}(\tau + 1)$ from $T^{eq}(\tau)$ and the $V_i(\tau + 1)$. Given the $V_i(\tau + 1)$, we obtain the $f_i(\tau + 1)$ from Eq. 10 and insert the results into Eqs. 11; also substituted into Eqs. 11 is $T^{eq}(\tau + 1)$ from Eq. 13. The resulting N expressions for the λ_i are then substituted into Eq. 12, and that equation is solved for $\lambda_s(\tau + 1)$. The λ_s itself can be plotted as a function of τ, or it can be substituted back into Eq. 13 and the tension increments can be stored in a computer disk file for later access. This sequence of points is treated like the actual data files and the resulting power density spectrum of force fluctuations as well as the magnitude of fluctuations are obtained. All computations have been performed on a Data General Eclipse S/200 computer (Data General Corp., Southboro, Mass.). Since the amount of memory space necessary to remember all N distortion distributions is very large, intermediate results after each time step Δt have been stored in sequential files on the disk and accessed later as required. The amount of time necessary for calculations is large (e.g., with 500 cross-bridges and 5 half-sarcomeres it is 35 s/time step); nevertheless, dt was fixed at 2 ms to allow for good resolution of tension-time curves.

The assignment of numerical values to the pertinent parameters of the model determines the dynamic characteristics of the model muscle as well as the absolute magnitude of T^{eq}. In computations k was taken as 1.5 pN/nm (22). k_s for the transducer arm was calculated to be 8 pN/nm but in calculations a value of 30 pN/nm was used to allow for a possible contribution by muscle series elasticity. The rate constants $f'(x)$ and $g'(x)$ were sufficiently small to have no influence on the results, while $f(x)$ and $g(x)$ were equal to $\frac{1}{10}$ of the values assigned to them by Julian (23) for the case of intact frog muscle at 0°C. Thus with $h = 10$ nm (8):

$$\begin{aligned} x < 0 \quad & f(x) = 0 \quad ; \quad g(x) = 39.2\,s^{-1}; \\ 0 \le x \le 10 \quad & f(x) = 8.1\,x\,s^{-1}; \quad g(x) = 1.9\,x\,s^{-1}; \\ 10 < x \quad & f(x) = 0 \quad ; \quad g(x) = 1.9\,x\,s^{-1}. \end{aligned} \tag{14}$$

In this way both the maximum velocity of shortening $V_{max} = 2h[f(h) + g(h)]$ and the maximum cross-bridge turnover rate $R_{max} = 0.5\,f(h)h/S_A$ assume $\frac{1}{10}$ of their 0°C frog muscle value. Here $S_A = 37.5$ nm as in ref. 22. The ratio of $\frac{1}{10}$ for the speeds of glycerinated rabbit fibers at room temperature and intact frog muscle at 0°C is close to that experimentally observed (24).

Results of Calculations

The representative power spectra for two sizes of cross-bridge populations with a fixed number of half-sarcomeres, and for a different number of half-sarcomeres with a fixed number of cross-bridges, are shown in Fig. 10. The spectra pertain to the flat part of the tension curves only, i.e., for 0.1 s $< t <$ 1.124 s. Within the limited range of populations explored we could not find evidence for a systematic effect of number of cross-bridges and half-sarcomeres on the shape of the power spectrum. The computed spectra rarely showed secondary maxima at higher frequencies, and the area under such peaks was always very much smaller than the area under the low frequency peak.

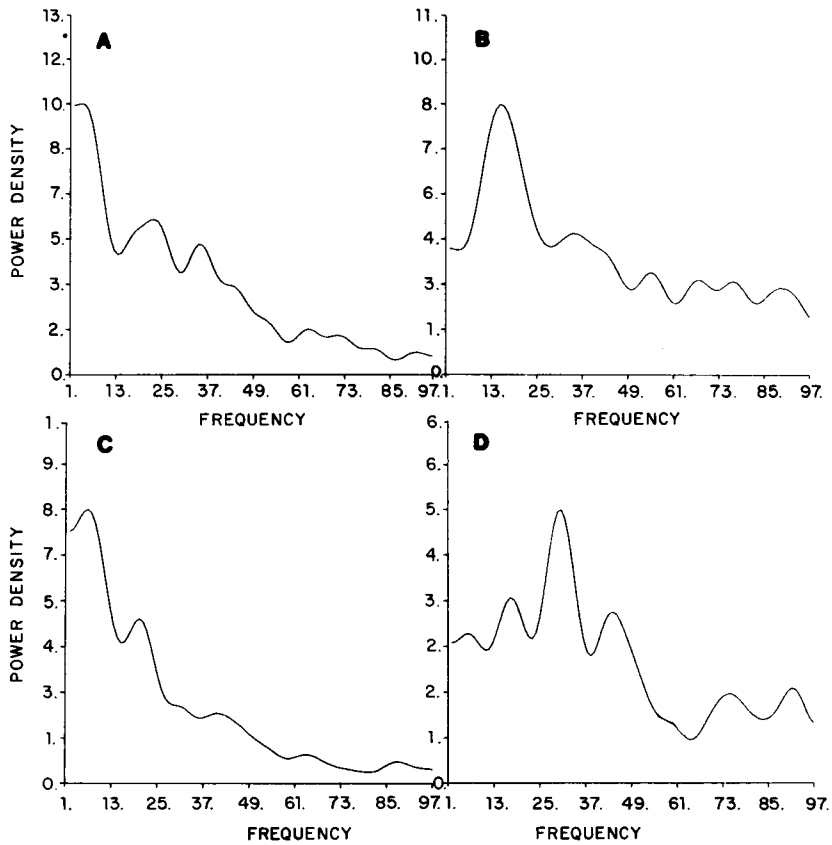

FIGURE 10 Examples of power spectra for a multicomponent muscle model with different number of cross-bridges and half-sarcomeres. Only smoothed spectra are shown; Bartlett window width was 256. A, B, C, and D correspond to 512, 512, 1,024, and 1,024 cross-bridges and 2, 10, 2, and 10 half-sarcomeres, respectively. Stiffness of transducer arm was 30 pN/nm, time step 0.002 s. Horizontal scale: 0.5 Hz/bin. Vertical scale in arbitrary units.

Table II summarizes results of some of the calculations. The normalized average force T^{eq} and its rms fluctuation apply only for 0.1 s $< t <$ 1.124 s. T^{eq} can be directly compared with Brokaw's value for isometrically held muscle comprising one half-sarcomere only (22). The size of the individual mechanochemical "impulse" force (25) is larger by a factor of about five, because on the average only one in about five cross-bridges is attached at any time. The equivalent stiffness of the tension generating unit k_1 is the normalized stiffness of the first half-sarcomere at the time that muscle tension equals T^{eq} and is given here as an example. Fig. 11 and Table II emphasize the important features of the model: namely, that the absolute fluctuation increases as the square root of the number of cross-bridges, and within the range investigated, it appears to decrease as a log of the number of half-sarcomeres (cf. Eq. 3). Thus, it is advantageous to work with a short muscle fiber; the lower limit of length, set by the mounting procedure, was about 1 mm.

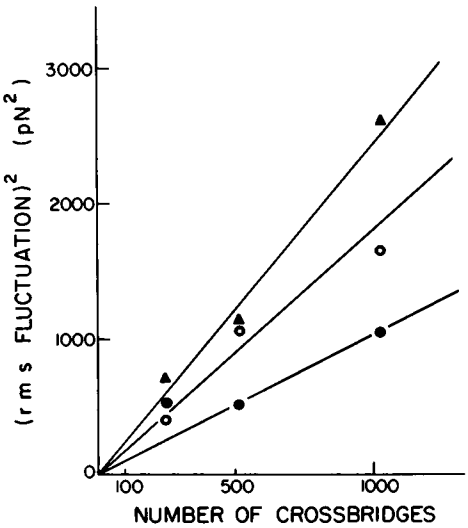

FIGURE 11 Absolute rms tension fluctuation as a function of the number of cross-bridges. Number of half-sarcomeres fixed at Δ, 2; o, 10; and •, 20.

DISCUSSION

The experiments described above reveal, in active but not in rigor or relaxed muscle, the existence of tension fluctuations composed of low-frequency components. These tension fluctuations probably result from the fluctuation in operation of the cross-bridges attached at any time. The kinetic parameters obtained from such experiments should be the same as those determined from isometric or isotonic quick-release experiments (26). For this purpose the advantage of the present method would be that the

TABLE II

MEAN ISOMETRIC FORCE, RELATIVE RMS FLUCTUATION, AND EQUIVALENT STIFFNESS FOR MULTICOMPONENT MUSCLE MODEL

n	N	T^{eq}	$<\delta T^{eq2}>^{1/2}$	k_1
		pN	*pN*	*pN/nm*
256	2	1.615	0.103	0.279
256	10	1.701	0.079	0.327
256	20	1.666	0.096	0.300
512	2	1.713	0.067	0.299
512	10	1.655	0.066	0.308
512	20	1.663	0.043	0.316
1,024	2	1.669	0.050	0.275
1,024	10	1.747	0.040	0.334
1,024	20	1.759	0.032	0.316

n and N denote number of cross-bridges and half-sarcomeres, respectively. T and $<\delta T^2>^{1/2}$ are the mean force and the rms force fluctuation per cross-bridge. k_1 is the equivalent stiffness per cross-bridge of the first half-sarcomere in the muscle, shown for comparative purpose. Transducer arm stiffness was fixed at 30 pN/nm, time step dt at 0.002 s. Average is of 512 steps starting at t = 0.100 s.

system does not have to be perturbed away from the equilibrium, a process that in certain systems could produce an error. The purpose of the model simulating the behavior of multicomponent muscle was to estimate the character of the power spectrum of force fluctuations and to compare computed spectra with the experimental frequency distributions. The good qualitative agreement between the two supports the idea that the observed fluctuations indeed arise from the temporal variations in the operation of attached cross-bridges. In this context, variations in the operation imply both the fluctuations in the number of attached cross-bridges and the fluctuations due to the fact that different attached cross-bridges are stretched to different extents, thus making different contributions to the tension. An apparent decrease in the fluctuations' amplitude with an increase in the number of half sarcomeres is not easily predicted a priori. The size of our computer limited our calculations to a relatively small number of sarcomeres and of cross-bridges per sarcomere. Thus we did not have a very wide range of "data" on which to develop our empirical equation, and estimates from this equation can be expected to be rough, particularly at very small and very large values of N. Nevertheless an order-of-magnitude comparison between estimated and observed fluctuations may be of interest: Knowing the tension generated by a 1-mm length of an extracted fiber, we can estimate that $N \sim 400$ and $n \sim 10^6$. Substituting into Eq. 3, we find that $<\delta d^2>^{1/2} \simeq 64$ nm. Using our calibration constant of 200 counts s^{-1} nm^{-1}, and assuming 50 bins s^{-1}, we can expect an rms fluctuation of 256 counts/bin. Experimental counting rates range from 10^4 to 4×10^5 counts/s, so the statistical fluctuations range from 14 to 89 counts/bin. The ratio of fluctuations varies between 3 and 18, larger than what we observed (Table I). This discrepancy may result in part from some deterioration of the preparation in the course of experimentation (as suggested by decreasing tension and tension recovery from quick release), but may also arise from an inadequate N-dependence in Eq. 3. With all the uncertainties in this order-of-magnitude calculation, the comparison is not upsetting.

A typical observed fluctuation (e.g., exp. 32 of Table I) constitutes 0.0033% of the total muscle tension. In practice the observed fluctuations are expressed as fractions of the width of the field of view defined by the field diaphragm. This increases the relative fluctuation by a factor of 100.

The range of frequencies observed in the present experiments is certainly not inconsistent with the rate of ATP splitting by actomyosin in solution. Under the conditions of saturation of myosin by actin, Lin and Morales reported the rate of 1 Hz for rabbit actomyosin ATPase at room temperature (27).

It is important to emphasize that one cannot at this point absolutely exclude the possibility that both the increase in fluctuation magnitude and the broadening of the power spectrum reported here for contracting muscle are artifacts associated with the experimental procedure. Artifacts may result from the filtering imposed on the data, i.e., fitting the experimental points with a straight line—a procedure necessary to eliminate the drift in muscle tension. Even though a straight line fit is obviously a good one (Fig. 6), there was no case in the present series of experiments when the tension creep was completely absent and the fit unnecessary. Two considerations how-

ever, suggest that this is not the case. Firstly, the histograms of fluctuations (e.g., Fig. 7B) were quite symmetrical, indicating that the linear fit to the data is justified. Any systematic departure from linearity would result in asymmetry of the histogram of the type illustrated in Fig. 7 A. Secondly, Table I shows that the drift rate and the increase in fluctuations were not correlated, and so suggests that the two are not causally related. Another possible source of artifacts is that the fluctuations may not arise from the variations in the number of attached cross-bridges but from microscopic damage or breakage of myofibrils unable to support their own tension. However, at the levels of tension developed by our preparations (<30 g/cm^2) such a possibility seems rather unlikely.

We are indebted to Mr. A. Schweitzer for illuminating discussions, for help in constructing the experimental apparatus, and for expert advice in computer programming, and to Dr. R. Mendelson for the discriminator-scaler part of our electronic circuitry. Thanks are also due to Dr. W. A. Hagins, who first called to the attention of one of us (M.F.M.) the utility of fluctuation analysis in studying cycling phenomena. Several friends kindly read this manuscript and were responsible for several improvements: Prof. C. Brokaw, Dr. W. A. Hagins, Dr. W. Halpern, and Dr. T. L. Hill.

This research was supported by the U.S. Public Health Service grants HL-16683 and HL-06285, National Science Foundation grant PCM-75-22698, and American Heart Association grant CI-8.

Received for publication 6 June 1977 and in revised form 4 August 1977.

REFERENCES

1. ELSON, E. L., and D. MAGDE. 1974. Fluorescence correlation spectroscopy. I. Conceptual basis and theory. *Biopolymers.* **13**:1–27.
2. MAGDE, D., E. L. ELSON, and W. W. WEBB. 1974. Fluorescence correlation spectroscopy. II. An experimental realization. *Biopolymers.* **13**:29–61.
3. KATZ, B., and R. MILEDI. 1972. The statistical nature of the acetylcholine potential and its molecular components. *J. Physiol. (Lond.).* **224**:665–699.
4. CARLSON, F. D., R. E. BONNER, and A. FRASER. 1972. Intensity fluctuation autocorrelation studies on resting and contracting frog's sartorius muscle. *Cold Spring Harbor Symp. Quant. Biol.* **37**:389–396.
5. BONNER, F. R., and F. D. CARLSON. 1975. Structural dynamics of frog muscle during isometric contraction. *J. Gen. Physiol.* **65**:555–581.
6. CARLSON, F. D. 1975. Structural fluctuations in the steady state of muscular contraction. *Biophys. J.* **15**:633–649.
7. JACKSON, J. L., and A. OPLATKA. 1974. A mechanochemical theory of fluctuations in muscles. *Biorheology.* **11**:315–322.
8. HUXLEY, A. F. 1957. Muscle structure and theories of contraction. *Prog. Biophys. Biophys. Chem.* **7**:255–311.
9. HILL, T. L. 1975. Theoretical formalism for the sliding filament model of contraction of striated muscle. *Prog. Biophys. Mol. Biol.* **29**:105–159.
10. CHEN, Y., and T. L. HILL. 1973. Fluctuations and noise in kinetic systems. *Biophys. J.* **13**:1276–1295.
11. BOREJDO, J., and A. OPLATKA. 1976. Tension development in skinned glycerinated rabbit psoas fiber segments irrigated with soluble myosin fragments. *Biochim. Biophys. Acta.* **440**:241–258.
12. BOREJDO, J., and S. PUTNAM. 1977. Polarization of fluorescence from single skinned glycernated rabbit psoas fibers in rigor and relaxation. *Biochim. Biophys. Acta.* **459**:578–595.
13. SCHAWARTZ, N., and L. SHAW. 1975. Signal Processing, Discrete Spectral Analysis, Detection and Estimation. McGraw-Hill Book Company, New York.

14. RABINER, L. R., and B. GOLD. 1975. Theory and Applications of Digital Signal Processing. Prentice-Hall, Inc., Englewood Cliffs, N.J.
15. PAPOULIS, A. 1965. Probability, Random Variables, and Stochastic Processes. McGraw-Hill Book Company, New York. 560–561.
16. LANDAU, L. D., and F. M. LIFSHITZ. 1960. Mechanics. Pergamon Press, Oxford.
17. FEYNMAN, R. P., R. B. LEIGHTON, and M. SANDS. 1968. The Feynman Lectures on Physics. Addison-Wesley Publishing Co., Inc., Reading, Mass.
18. SANDOW, A., and G. E. MAURIELLO. 1953. Fusion frequency, and kinetics of active state in muscular tetanus. *Fed. Proc.* **12**:123–124.
19. GORDON, A., A. F. HUXLEY, and F. J. JULIAN. 1966. The variation in isometric tension with sarcomere length in vertebrate muscle fibers. *J. Physiol. (Lond.).* **184**:170–192.
20. BOREJDO, J., and A. SCHWEITZER. 1977. Tension measurements in isolated myofibrils. *J. Mechanochem. Cell Motility.* In press.
21. HILL, T. L., E. EISENBERG, Y. CHEN, and R. J. PODOLSKY. 1975. Some self consistent two state sliding filament models of muscle contraction. *Biophys. J.* **15**:335–372.
22. BROKAW, C. J. 1976. Computer simulation of movement-generating cross-bridges. *Biophys. J.* **16**: 1013–1027.
23. JULIAN, F. J. 1969. Activation in a skeletal muscle contraction model with a modification for insect fibrilar muscle. *Biophys. J.* **9**:547–570.
24. WISE, R. M., J. F. RONDINONE, and F. M. BRIGGS. 1971. Effect of calcium on force-velocity characteristics of glycerinated skeletal muscle. *Am. J. Physiol.* **221**:973–979.
25. OPLATKA, A. 1972. On the mechanochemistry of muscular contraction. *J. Theor. Biol.* **34**:379–403.
26. HUXLEY, A. F., and R. M. SIMMONS. 1971. Proposed mechanism of force generation in striated muscle. *Nature (Lond.).* **233**:533–538.
27. LIN, T., and M. F. MORALES. 1977. Application of a one-step procedure for measuring inorganic phosphate in the presence of proteins. *Anal. Biochem.* **77**:10–17.
28. WEBER, A., and J. M. MURRAY. 1973. Molecular control mechanisms in muscle contraction. *Physiol. Rev.* **53**:612–673.